Magnetic Resonance Imaging 55 (2019) 93–102

Contents lists available at ScienceDirect

Magnetic Resonance Imaging

journal homepage: www.elsevier.com/locate/mri

Original contribution

Characterization of prostate cancer with MR spectroscopic imaging and diffusion-weighted imaging at 3 Tesla

Yousef Mazaheri[a,b,*], Amita Shukla-Dave[a,b], Debra A. Goldman[c], Chaya S. Moskowitz[c], Toshikazu Takeda[d], Victor E. Reuter[d], Oguz Akin[b], Hedvig Hricak[b]

[a] Department of Medical Physics, Memorial Sloan Kettering Cancer Center, New York, NY, USA
[b] Department of Radiology, Memorial Sloan Kettering Cancer Center, New York, NY, USA
[c] Department of Epidemiology and Biostatistics, Memorial Sloan Kettering Cancer Center, New York, NY, USA
[d] Department of Pathology, Memorial Sloan Kettering Cancer Center, New York, NY, USA

ARTICLE INFO

Keywords:
ADC = apparent diffusion coefficient
DWI = diffusion-weighted imaging
PZ = peripheral zone
ROI = region of interest
3D = three-dimensional
MR spectroscopic imaging MRSI

ABSTRACT

Purpose: To retrospectively measure metabolic ratios and apparent diffusion coefficient (ADC) values from 3-Tesla MR spectroscopic imaging (MRSI) and diffusion-weighted imaging (DWI) in benign and malignant peripheral zone (PZ) prostate tissue, assess the parameters' associations with malignancy, and develop and test rules for classifying benign and malignant PZ tissue using whole-mount step-section pathology as the reference standard.

Methods: This HIPAA-compliant, IRB-approved study included 67 men (median age, 61 years; range, 41–74 years) with biopsy-proven prostate cancer who underwent preoperative 3 T endorectal multiparametric MRI and had ≥1 PZ lesion > 0.1 cm^3 at whole-mount histopathology. In benign and malignant PZ regions identified from pathology, voxel-based choline/citrate, polyamines/choline, polyamines/creatine, and (choline + polyamines + creatine)/citrate ratios were averaged, as were ADC values. Patients were randomly split into training and test sets; rules for separating benign from malignant regions were generated with classification and regression tree (CART) analysis and assessed on the test set for sensitivity and specificity. Odds ratios (OR) were evaluated using generalized estimating equations.

Results: CART analysis of all parameters identified only ADC and (choline + polyamines + creatine)/citrate as significant predictors of cancer. Sensitivity and specificity, respectively, were 0.81 and 0.82 with MRSI-derived, 0.98 and 0.51 with DWI-derived, and 0.79 and 0.90 with MRSI + DWI-derived classification rules. Areas under the curves (AUC) in the test set were 0.93 (0.87–0.97) with ADC, 0.82 (0.72–0.91) with MRSI, and 0.96 (0.92–0.99) with MRSI + ADC.

Conclusion: We developed statistically-based rules for identifying PZ cancer using 3-Tesla MRSI, DWI, and MRSI + DWI and demonstrated the potential value of MRSI + DWI.

1. Introduction

Multi-parametric magnetic resonance imaging (MRI) of the prostate is increasingly being used in the detection, localization, staging, risk stratification and surveillance of untreated prostate cancer, as well as for guiding biopsies and interventions and assessing potential cancer recurrence [1]. In addition to T1- and T2-weighted anatomic MRI sequences, mp-MRI examinations incorporate one or more sequences that assess function or physiology—typically, dynamic contrast-enhanced MRI (DCE-MRI), which reflects vascularity and perfusion; diffusion-weighted MRI (DWI), which reflects restriction of water diffusion and thus corresponds to properties such as cellular density, membrane permeability and spacing between cells [2]; and/or, more rarely, proton MR spectroscopic imaging (MRSI), which shows changes in relative metabolite levels that occur in prostate cancer [3,4]. The use of MRSI in multi-parametric MRI studies is less common than the use of DCE-MRI or DWI, in part because it requires relatively long acquisition times and specialized expertise for optimal technical implementation and interpretation. However, MRSI is non-invasive and has generally been found to offer good specificity, which could complement the sensitivity offered by DWI. Furthermore, like DWI, it can provide an indication of tumor aggressiveness [5].

Proton MRSI studies of the prostate focus on citrate (Cit), creatine (Cre), choline (Cho), and polyamines (PA). Prostate cancer is

* Corresponding author at: Departments of Medical Physics and Radiology, Memorial Sloan Kettering Cancer Center, New York, NY, USA.
E-mail address: mazahery@mskcc.org (Y. Mazaheri).

https://doi.org/10.1016/j.mri.2018.08.025
Received 3 October 2017; Received in revised form 29 August 2018; Accepted 30 August 2018

characterized by elevated choline and decreased citrate and polyamines [6,7]. More than a decade ago, a zone-specific threshold-based system was developed for classifying prostate voxels in the peripheral zone as cancerous or benign at 1.5-Tesla (1.5 T) MRSI based on the Cho + PA + Cr/Cit ratio [8]. This approach was found to have high accuracy for prostate cancer localization, with moderate-to-excellent interobserver agreement [9]. Subsequently, a probability-based rule was developed for classifying voxels as malignant or benign at 1.5 T MRSI; with this rule, the level of polyamines was first scored on a scale of 0 (undetectable) to 2 (as high as or higher than the choline peak), and a score of 0 or 1 was considered to indicate malignancy; if the PA score was 2, then the Cho + PA + Cr/Cit ratio was evaluated [10]. The rule had 42% sensitivity and 85% specificity in a 667-voxel test set, and its sensitivity rose to 75% in voxels with > 90% malignancy [10].

Improvements in SNR and larger chemical shift dispersion, as well as improved pulse sequence designs, have motivated various groups to examine 3 T MRSI for the evaluation of the prostate [5,11,12]. The increased metabolic resolution available at 3 T is especially important if characterization of polyamine resonances is a component of the spectroscopic data analysis. Studies with high-resolution magic angle spinning (HR-MAS) MRS have shown that high-grade cancer tissue can be distinguished from low-grade cancer tissue by decreased concentrations of spermine (a polyamine) and citrate [13].

The added SNR available at 3 T, as compared to 1.5 T, can also improve the accuracy of tumor detection and staging by DWI—a technique that is now commonly included (with or without MRSI) in so-called “multiparametric” MRI studies of the prostate [14].

Some studies have examined the value of combining DWI and MRSI at 1.5 T for the identification of peripheral zone (PZ) prostate cancer: Reinsberg et al. found that the combination of DWI and MRSI (using Cho/Cit) performed significantly better than either technique alone, while we found the combination of DWI and MRSI (using Cho + PA + Cr/Cit) performed significantly better than MRSI but only slightly better than DWI alone [15,16]. However, to our knowledge, no prior study has presented a systematic approach for characterizing benign and malignant PZ with MRSI and DWI at 3 T. The aims of our study were to retrospectively measure metabolite ratios and apparent diffusion coefficient values for benign and malignant PZ tissue from 3-Tesla MRSI and DWI, assess their associations with malignancy, and develop and test rules for classifying benign and malignant PZ tissue using whole-mount step-section pathology as the reference standard.

2. Materials and methods

2.1. Study subjects

Our study was compliant with HIPAA and was approved by our institutional review board. It included 67 men (median age, 61 years; range, 41–74 years) with untreated, biopsy-proven prostate cancer. Between December 2008 and October 2011, patients who gave informed consent to be enrolled in this study to assess the value of 3 T MRSI of the prostate using a non-FDA-approved MRSI acquisition sequence underwent 3 T MRI, DWI, and MRSI. Twelve patients were excluded from the study: in two, the tumor was located only in the transition zone; in three, the index lesion was 0.1 cm^3 or smaller; and in six, the artifacts seen at MRSI (n = 6) or DWI (n = 1) precluded accurate evaluation (Fig. 1). The analysis presented here included those patients who subsequently underwent surgery and for whom whole-mount histopathology showing at least one PZ lesion larger than 0.1 cm^3 was available.

2.2. MR imaging

All MRI studies were performed on a 3 T unit (Signa HDX; GE Healthcare, Milwaukee, Wis). The unit was equipped with gradient coil designed to achieve 50-mT/m peak gradient amplitude at a slew rate of 150 T/m/s. A body coil was used for excitation. For signal reception, both a pelvic eight-channel phased-array coil and a commercially available balloon-covered expandable endorectal coil (Medrad, Warrendale, Pa, USA), inflated with barium sulfate (*E-Z*-EM, Inc., Lake Success, NY) to about 60–100 mL, were used.

The standard clinical prostate examination used included high-resolution images of the prostate and seminal vesicles obtained with an axial T1-weighted sequence (TR/TE = 600–883/7.1–11.4 msec), 5 mm slice thickness, 0-mm inter-slice gap, field of view [FOV] = 32 cm, acquisition matrix = 288 × 160, reconstruction matrix = 512 × 512 and transverse, coronal, and sagittal T2-weighted fast spin-echo sequences (TR/effective TE = 3800–6667/116–143.3 msec, echo train length = 24, 3 mm slice thickness, no inter-slice gap, FOV = 14–24 cm, acquisition matrix = 448 × 224, reconstruction matrix = 512 × 512).

2.3. Diffusion-weighted imaging

DW images were obtained by using single-shot spin-echo echo-planar imaging with a pair of rectangular gradient pulses along three orthogonal axes in transversal orientation to include the whole prostate. For these images, the orientation and location were prescribed exactly as they were for the transverse T2-weighted prostate images. Using both a pelvic phased-array coil and an endorectal coil, DW images were acquired with the following parameters: TR/TE = 3500–6800/74.1–86.2 msec; section thickness, 3 mm; no inter-slice gap; FOV, 12–16 cm; acquisition matrix = 128 × 128, reconstruction matrix = 256 × 256. Parallel imaging with a factor of 2 and fat suppression was used. The *b*-values were 0 and 1000 s/mm^2. The time required to acquire the DWI was 6–8 min.

2.4. Three-dimensional proton MR spectroscopic imaging

For MRSI studies, only the endorectal coil was used for signal reception. MRSI data were acquired with the acquisition software (PROSE; General Electric Medical Systems, Milwaukee, WI) provided by GE under a research agreement, with a HIPAA-compliant, IRB-approved protocol. Prescription selection was performed on axial T2-weighted images. In the PROSE sequence, spatial localization was achieved using the Point Resolved Spatial Selection (PRESS) technique. Outer volume saturation pulses were used to confine the PRESS selection to the shape of the prostate and to reduce unwanted water and lipid signal. The PRESS box was positioned to maximize coverage of the prostate and minimize periprostatic fat. Water and lipid signal were suppressed with dual-band spectral-spatial radiofrequency 180° pulses to excite the metabolites of interest in a volume encompassing the prostate while suppressing water and lipids [17]. Acquisition parameters were TR/TE = 1300/85 msec; NEX = 1; FOV = 11 × 5.5 cm^2, acquisition slice thickness = 6.9 mm, acquisition matrix = 12 × 8 × 8. The data was zero filled in both the phase- and slice-encoding direction. The reconstructed voxel size was 0.11 cm^3. To address *J*-modulation of the citrate signal measured at 3 T, the MLEV-PRESS sequence proposed by Chen et al. was used [18], which resulted in the citrate signal being upright at TE = 85 msec. The duration of MRSI data acquisition was about 17 min. The PRESS box was positioned on transverse T2-weighted images to maximize coverage of the prostate while minimizing inclusion of periprostatic fat. An automated shimming algorithm provided by the manufacturer was used. If necessary, further shimming was performed manually, to further reduce the line width.

2.5. Data processing and analysis

Spectral data were processed by using the manufacturer's post-processing software package. Processing included zero filling of the raw data in the superoinferior direction, Fourier transformation reconstruction, and spectral apodization with a 2-Hz Lorentzian function, baseline correction, peak registration, and alignment of spectroscopic

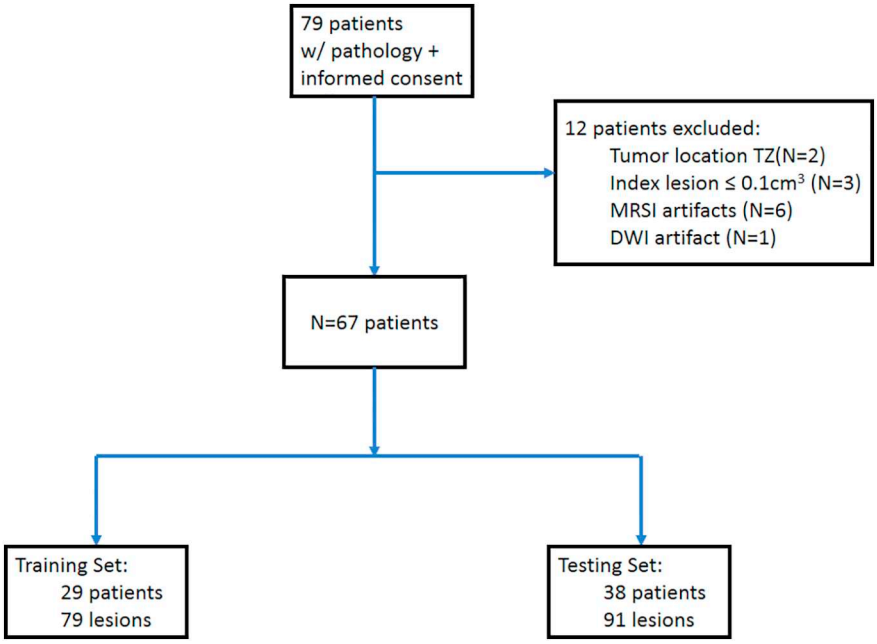

Fig. 1. A flowchart showing the number of patients/lesions included in the analysis.

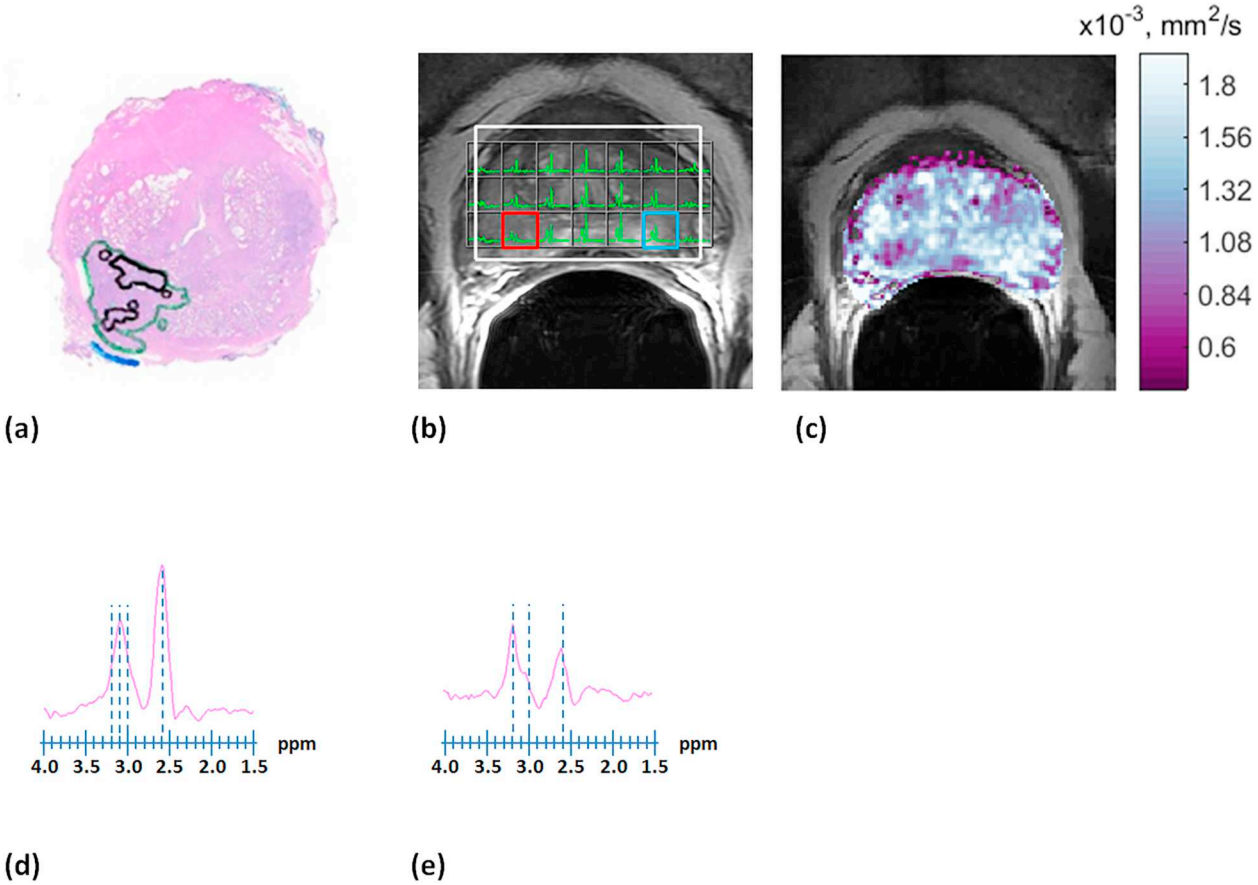

Fig. 2. (A) Whole-mount step-section histopathologic map (hematoxylin-eosin stain). (B) MR spectroscopic imaging grid superimposed on transverse T2-weighted MR image of the peripheral zone of the prostate of a 55-year-old patient with tumor located in the PZ (presurgical PSA level, 6.07 ng/mL; Gleason score, 7 [3 + 4]). (C) ADC map of same section as in (B), generated by using diffusion-weighted MR images. (D) A healthy voxel with high levels of citrate (Cit) and containing polyamine (PA) and creatine (Cr) signals. (E) A tumor voxel characterized by high levels of choline (Cho) levels and decreased levels of Cit and PA.

data to the transverse T2-weighted images. To estimate area under the metabolic peaks, a region centered at each peak was integrated. The chemical shifts for the peaks of the metabolites (measured as a downward frequency shift relative to water) are approximately 3.2, 3.1, 3.0, and 2.6 ppm for Cho, PA, Cre, and Cit [19]. The diameter of integration was as follows: for the integral of Cho the range was

Table 1
Distribution of patient characteristics.

		All	Testing	Training	p-Value
Age (years)	Median (range)	61.6 (41.5–74.7)	61.3 (46.7–74.7)	61.8 (41.5–74.2)	0.64
Time b/w MRI and surgery (days)	Median (range)	13 (0–442)	16 (1–442)	12 (0–363)	0.43
PSA (mg/DL)	Median (range)	5.0 (0.1–65.8)	4.9 (0.1–65.8)	5.1 (0.1–20.0)	0.80
Gleason score	6	11 (16.4)	7 (18.4)	4 (13.8)	0.74
	≥7	56 (83.6)	31 (81.6)	25 (86.2)	

Table 2
Median lesion-level MRSI and ADC characteristics.

	All	Testing	Training	p-Value
Choline/citrate	0.35 (0.10–2.39)	0.35 (0.10–2.39)	0.36 (0.14–1.02)	0.54
Polyamines/choline	0.93 (0.52–2.38)	0.91 (0.52–2.38)	0.94 (0.61–1.26)	0.26
Polyamines/creatine	0.86 (0.27–2.70)	0.89 (0.29–2.70)	0.83 (0.27–1.47)	0.11
MRSI ratio	0.85 (0.33–3.08)	0.82 (0.33–3.08)	0.87 (0.41–1.68)	0.21
ADC	1.32 (0.93–1.89)	1.31 (0.94–1.84)	1.32 (0.93–1.89)	0.82

Table 3
Diagnostic accuracy for the three decision trees based on the test set.

Variable	Sensitivity [95% CI; n]	Specificity [95% CI; n]
Optimal tree (MRSI only)	0.81 [0.66–0.91;42/52]	0.82 [0.66–0.93;32/39]
Optimal tree (DWI only)	0.98 [0.89–1;51/52]	0.51 [0.34–0.68;20/39]
Optimal tree (MRSI + DWI)	0.79 [0.64–0.89;41/52]	0.90 [0.76–0.97;35/39]

3.34–3.19 ppm, for the integral of PA the range was 3.19–3.12 ppm, for the integral of Cre the range was 3.12–2.97 ppm, for the integral of choline to creatine (Cho + PA + Cre), which includes the polyamines,

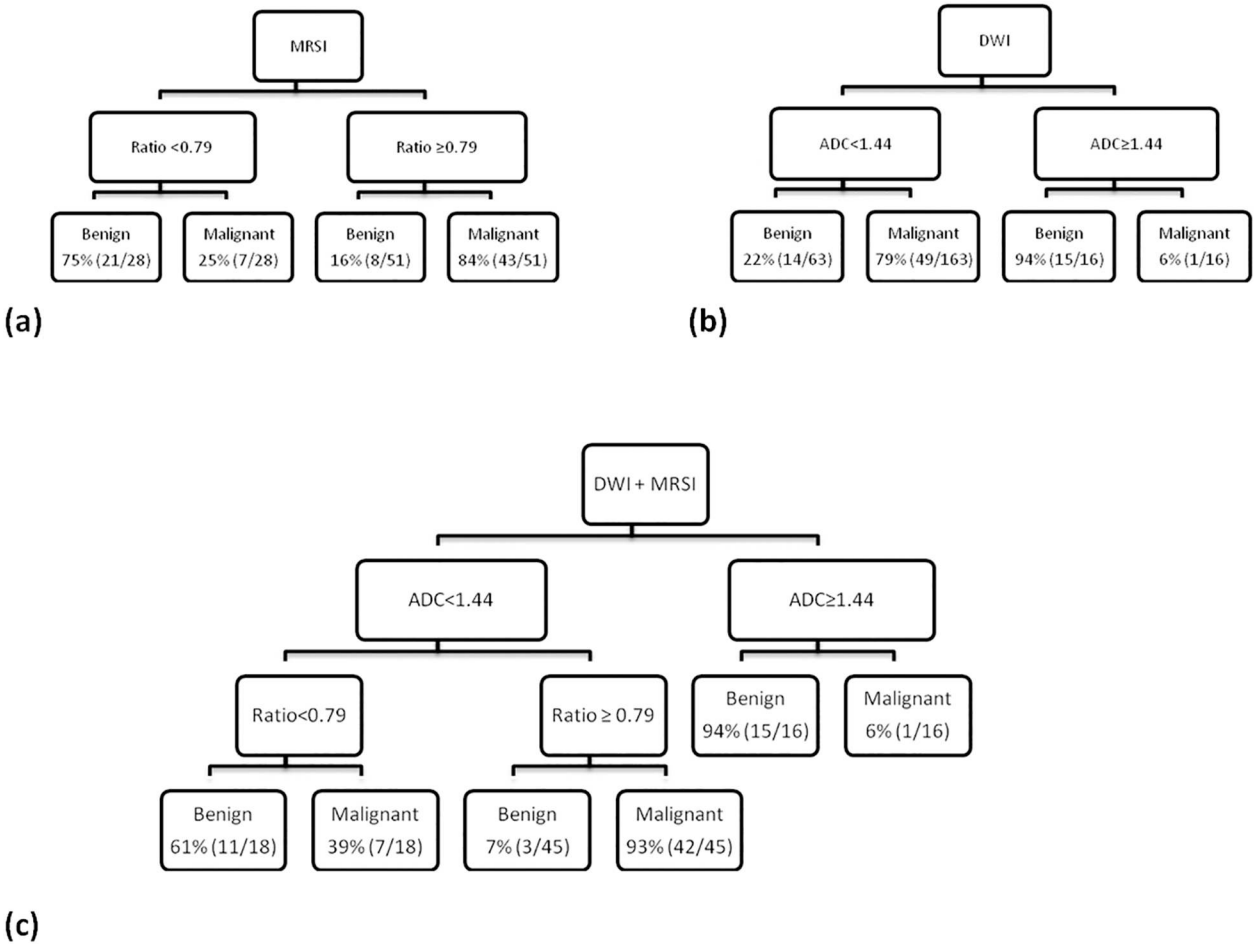

Fig. 3. (A) Recursive partition tree of MRSI. All MRSI parameters were entered into the recursive partitioning process. After partitioning and pruning, the only remaining split was the MRSI ratio. In this decision rule, the lesion was considered benign if the ratio was < 0.79 and malignant if the ratio was greater than or equal to 0.79. (B) Recursive partition tree of DWI. ADC was entered into a recursive partitioning tree as the only parameter. Based on this process, a lesion was considered malignant if ADC was $< 1.44 \times 10^{-3}$ mm^2/s and considered benign if ADC was $> 1.44 \times 10^{-3}$ mm^2/s. (C) Recursive partition tree of MRSI + DWI. After recursive partitioning and pruning, both ADC and the MRSI ratio remained as splits in the decision tree. If ADC was greater than or equal to 1.44×10^{-3} mm^2/s, the lesion was considered benign. If the ADC was $< 1.44 \times 10^{-3}$ mm^2/s, then the MRSI parameter was used to create the split. If the MRSI ratio was < 0.79, the lesion was considered benign. If the MRSI ratio was greater than or equal to 0.79, the lesion was considered malignant.

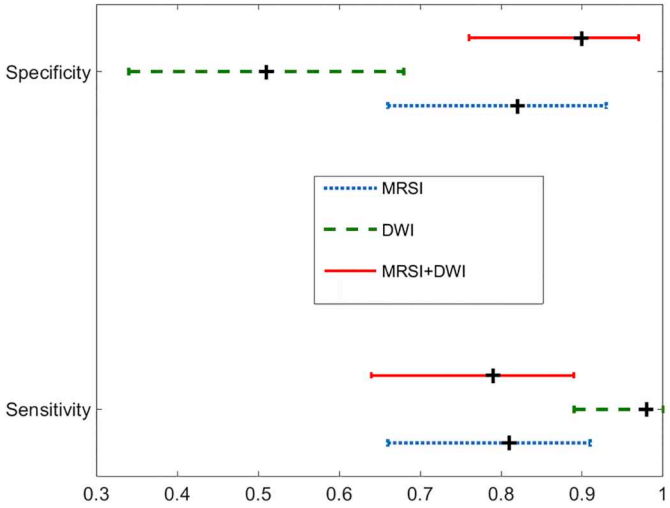

Fig. 4. Graph of sensitivity and specificity of optimal decision tree results on test dataset.

Table 4
Results of univariate generalized estimating equations (training set).

		OR	95% CI	p-Value
Cancerous	Choline/citrate	34.72	[2.10 – 572.97]	**0.013**
	Polyamines/choline	0.50	[0.03 – 7.79]	0.62
	Polyamines/creatine	2.63	[0.52 – 13.39]	0.24
	MRSI ratio[a]	1.08	[1.03 – 1.13]	< **0.001**

[a] Units of MRSI ratio have been adjusted so that the increment on the odds ratio is 0.01.

the range was 3.34–2.97 ppm, and for the integral of Cit the range was 2.86–2.57 ppm (Fig. 2). The following metabolic ratios were measured: Cho/Cit, PA/Cho, PA/Cre, and Cho + PA + Cre/Cit (hereafter we will simply refer to this last ratio as the MRSI ratio, in accordance with the literature). Voxel-wise ADC maps were generated on workstations provided by the manufacturer (Advantage Windows; GE Medical Systems) assuming a mono-exponential signal decay.

2.6. Pathologic evaluation and image correlation

The transverse T2-weighted images were used to pair imaging data (MRSI and DW images) and the pathologic step-section slices. Anatomical landmarks used for matching imaging to pathology include the presence of urinary bladder and seminal vesicle tissue in superior slices, the slice with the largest diameter and progressive changes in the diameter of the slices, the thickness of the peripheral zone, the position of the pseudocapsule, and the presence, size, and shape of the transition zone.

Using both pathology maps and MR images, MRSI voxels in the tumor were identified, and metabolic information was extracted from each voxel. Circular regions-of-interest (ROIs) outlining the tumors were placed on ADC maps. Additionally, voxels (from the MRSI maps) and ROIs (placed on ADC maps) were positioned in a location in the PZ where there was no indication of prostate cancer (if possible on the opposite side of the prostate), avoiding regions containing post-biopsy hemorrhage, prostate capsule, or the urethra. Areas containing post-biopsy hemorrhage or prostate capsule were avoided.

Areas assigned Gleason grade 3 was outlined in green, and areas assigned Gleason grade 4 (and above) were outlined in black. The fraction (expressed as a percentage) of the area of Gleason grade ≥4 disease to the total area of the lesion was measured on histopathology maps. The values ranged from 0 (for 3 + 3 lesions) to 100% for (≥4 + 4 lesions).

2.7. Statistical analysis

As DWI characteristics are only available at the lesion level, the average of MRSI voxel-level data was used for each lesion. We compared the clinical and imaging characteristics between the training and test sets using Fisher's exact test and the Wilcoxon Rank Sum test where appropriate. We ran parallel analyses using two methods. In the training set, classification and regression tree (CART) analysis was used to generate a rule for separating cancerous from benign lesions based on MRSI values. The results were subsequently analyzed against generalized estimating equations (GEE).

For CART analyses, recursive partitioning was first applied to the MRSI-measured ratios from the training set, and the tree was optimized using cross-validation (N = 10) and cost-complexity pruning. Recursive partitioning splits the data into binary groups using the quantities until either all groups contain the same members (i.e. all cancer or all benign) or a group has too few members to split any further. The Gini index was used to grow the tree, and we set the minimum bucket size to 10 lesions. The optimal tree was displayed in a decision tree plot and the decision rule created based on the tree branches. The decision rule was applied to the test set, and the sensitivity and specificity of the predicted value compared to the true cancer status were calculated. Bootstrap adjusted 95% confidence intervals (CI) were provided to account for multiple lesions within the same patients.

A separate tree was built for DWI alone using the methods above, and the sensitivity and specificity of DWI were calculated using the test set. Recursive partitioning was then applied to DWI and the MRSI-measured ratios from the MRSI-only tree using the methods above.

Univariate analyses examining the relationships between cancer status and each of the MRSI-measured ratios were performed using generalized estimation equations with logit link functions and independent working correlation matrices, accounting for multiple lesions within the sample patient. Univariate logistic regression was used to evaluate associations between the likelihood of cancer and MRSI-measured ratios using odds ratios. Variables significant at the 0.05 level were examined with bootstrapped (N = 200) areas under the curves (AUC) using the test set. A GEE model with DWI alone was calculated on the training set, and the MRSI-measured ratio with the highest AUC was added to this model. Receiver operating characteristic curves and the corresponding AUCs were estimated non-parametrically for the identification of cancer for the test set. The Wald test was conducted on each of the parameters within these models on the test set to assess the added value of the MRSI parameter. Additionally, the AUCs for MRSI, DWI and MRSI + DWI were examined using the test dataset, but no formal testing of these models was conducted, as comparison between two AUCs in a nested model is not appropriate [20].

The relationships between MRSI and DWI and percentage of Gleason grade ≥4 disease within lesion was examined using GEE with identity link functions and independent working correlation matrices. All patients and lesions were included in this analysis.

All statistical analyses were performed using SAS 9.4 (The SAS Foundation, Cary, NC) and Cran R 3.2.1 with the “rpart,” “rpart.plot,” “rattle,” and “caret” (The R Project).

3. Results

Initially, the analysis was set to have half the patients in the training and half the patients in the test sets. The dataset was randomly split into training and test sets at the patient level using PROC PLAN within SAS 9.4. Twenty-nine of the 57 patients (79 lesions) were used for the training set. Initially, 28 patients (68 lesions) were included in the test set. After the randomization was done and the training analyses were run, data became available for an additional 10 patients. These ten patients (22 lesions) were added to the test set, making the total 38 patients with 91 lesions. Based on comparison with histopathology, 50 (49%) malignant lesions were used in the training set and 52 (51%)

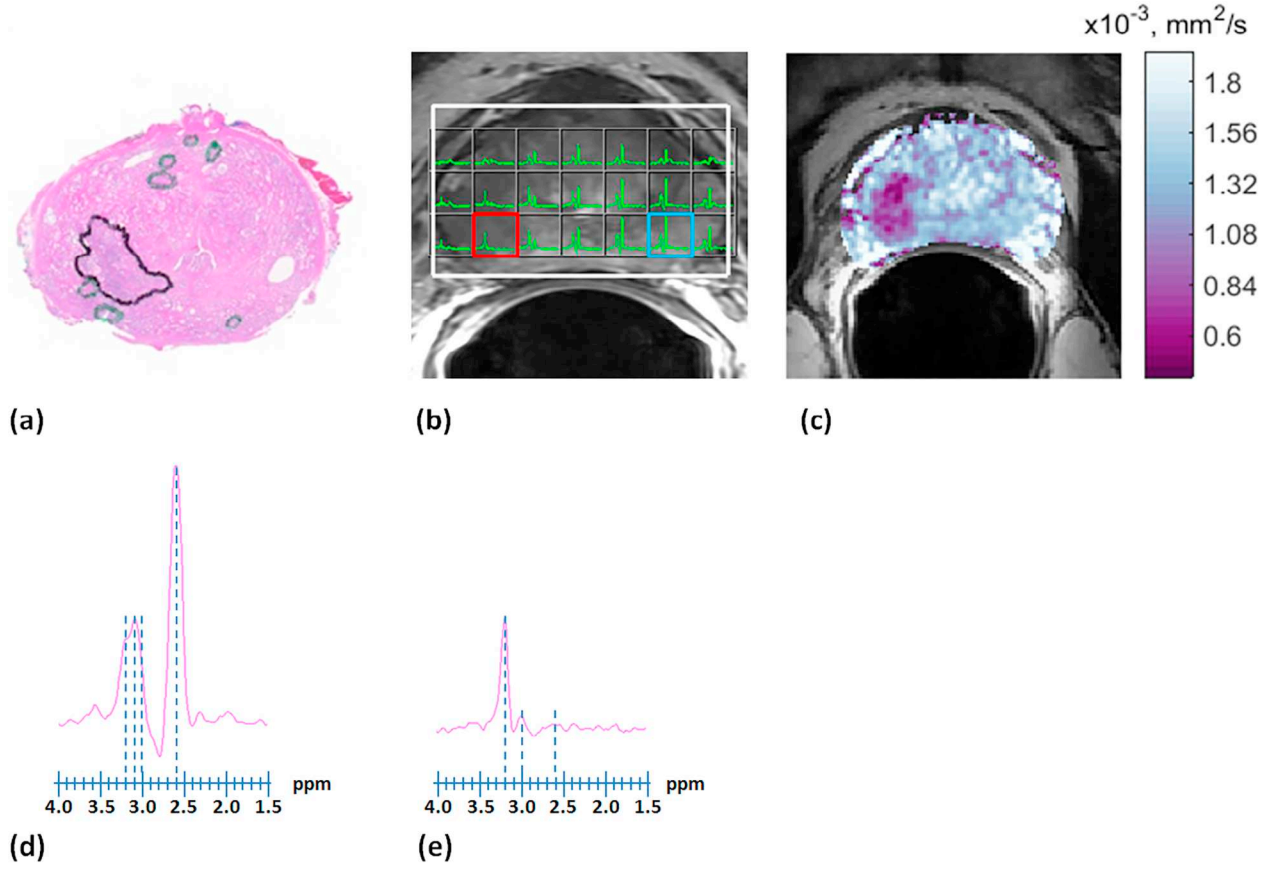

Fig. 5. MRI/MRSI from a 58-year-old patient with tumor located in the PZ (presurgical PSA level, 4.57 ng/mL; Gleason score, 7 [4 + 3]) (A) Whole-mount step-section histopathologic map (hematoxylin-eosin stain). (B) MR spectroscopic imaging grid superimposed on transverse T2-weighted MR image. (C) ADC map of same section as in (B). (D) A healthy-appearing voxel and (E) a PZ tumor voxel in the PZ.

malignant lesions were used in the test set. For each patient, a benign ROI was also identified (29 ROIs for the training set, 38 ROIs for the test set).

Of the 67 patients, eleven (16.4%) had a Gleason sum of 3 + 3, 38 (56.7%) had a Gleason sum of 3 + 4, 13 (19.4%) had a Gleason sum of 4 + 3, and five (7.5%) had a Gleason score of 8 or greater at surgery. The median Gleason score at surgical pathologic examination was 7 (range, 6–9). The median serum PSA level for the cohort was 5 ng/mL (range, 0.1–65.8 ng/mL) (Table 1).

Table 2 summarizes the mean MRSI and DWI characteristics for the benign and malignant lesions of all patients in the test and training sets. No significant differences were found between the training and test sets.

All MRSI parameters were entered into the model. The final tree only contained the MRSI ratio (Fig. 3a). The lesion was considered benign if the ratio was < 0.79 and malignant if the ratio was greater than or equal to 0.79.

In the DWI only tree (Fig. 3b), a lesion was considered malignant if ADC was $< 1.44 \times 10^{-3}$ mm^2/s and benign if ADC was greater than or equal to 1.44×10^{-3} mm^2/s.

In the third tree, both ADC and the MRSI ratio remained as splits (Fig. 3c). If the ADC was greater than or equal to 1.44×10^{-3} mm^2/s, the lesion was considered benign. If the ADC was $< 1.44 \times 10^{-3}$ mm^2/s, then the MRSI ratio was incorporated. If the MRSI ratio was < 0.79, the lesion was considered benign. If the MRSI ratio was greater than or equal to 0.79, the lesion was considered malignant.

The sensitivities and specificities [95% CI] for the test set based on the trees above are summarized in Table 3 (Fig. 4). The ADC-only tree had the highest sensitivity (0.98, 95%CI: 0.89–1.00) but poor specificity (0.51, 95%CI: 0.34–0.68). When MRSI ratio was incorporated, the specificity rose to 0.90 (95% CI: 0.76–0.97), though the sensitivity dropped to 0.79 (95% CI: 0.64–0.89). Ultimately, the MRSI + DWI tree had the highest combined sensitivity and specificity.

Univariate analyses for each of the MRSI-measured ratios of the training set found that Cho/Cit and MRSI ratio were associated with malignancy (Table 4). Figs. 5–6 shows examples of tumor that was clearly depicted on MRI, DWI and MRSI. The AUCs [95% CI] derived with the significant variables from the training and test sets are given in Table 5. For the test set, the AUCs were 0.93 [0.87–0.97] using ADC and 0.82 [0.72–0.91] using MRSI ratio; MRSI + DWI had the highest AUC, at 0.96 [0.92–0.99].

In the test set, ADC alone was a significant predictor of cancer (OR: 0.83, 95% CI: 0.76–0.91, p < 0.001). When MRSI ratio was added to the model, ADC remained significant (OR: 0.84, 95% CI: 0.77–0.91, p < 0.001), and MRSI ratio was also significantly associated with cancer status (OR: 1.06, 95% CI: 1.03–1.10, p < 0.001); this suggests that MRSI ratio adds value to ADC alone.

In univariate analysis, all MRSI parameters and ADC were significantly associated with percentage of Gleason grade ≥4 tumor. Lesions with higher Cho/Cit, PA/Cre, and MRSI ratio and lower PA/Cho and ADC (negative Beta values) were more likely to have a greater percentage of Gleason grade ≥4 tumor (Table 6). Fig. 7 are scatter plots of mean MRSI parameters (Fig. 7a) and mean ADC (Fig. 7b) and the line of best fit versus percentage of Gleason grade 4 tumor for all lesions in the analysis. The scatter plots suggest variability in the data but the trends are consistent with the univariate analysis.

4. Discussion

Two prior studies at 1.5 T examined prostate cancer identification in the PZ with MRSI + DWI [15,16]. We built on those studies by

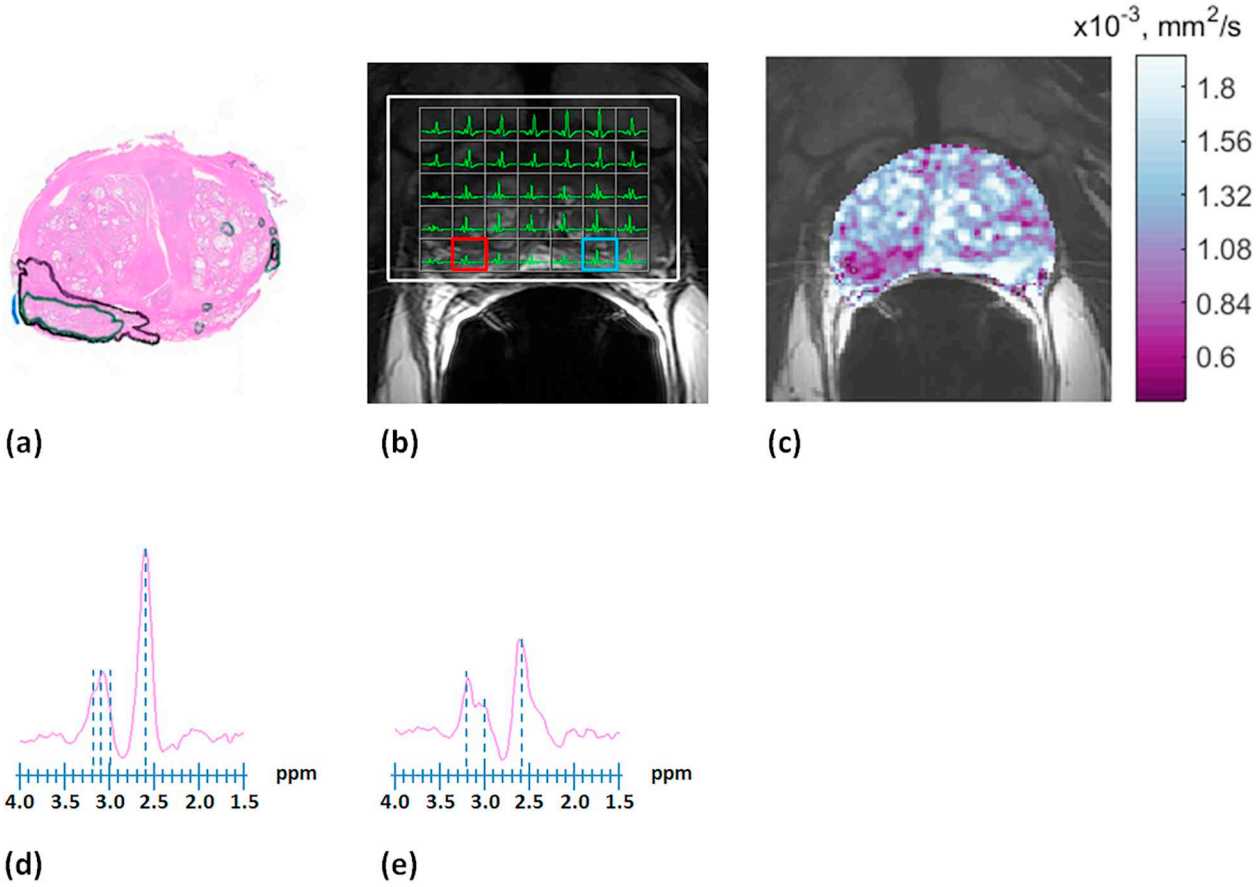

Fig. 6. (A) Whole-mount step-section histopathologic map (hematoxylin-eosin stain). (B) MR spectroscopic imaging grid superimposed on transverse T2-weighted MR image of the peripheral zone of the prostate of a 74-year-old patient with tumor located in the PZ (presurgical PSA level, 14.7 ng/mL; Gleason score, 7 [4 + 3]). (C) ADC map of same section as in (B). (D) A healthy-appearing voxel and (E) a PZ tumor voxel in the PZ.

Table 5
AUC values of variables.

Training			Testing		
Variable	AUC	(95% CI)	Variable	AUC	(95% CI)
Choline/citrate	0.62	(0.49–0.76)	ADC	0.93	(0.87–0.97)
MRSI ratio	0.84	(0.74–0.93)	MRSI ratio	0.82	(0.72–0.91)
ADC	0.86	(0.77–0.92)	ADC + MRSI ratio	0.96	(0.92–0.99)

Table 6
Univariate relationships between MRSI and ADC parameters and Gleason grade ≥4 percentage for all patients.

		Beta	95%	CI	p-Value
% Gleason grade 4	Choline/citrate	46.74	[19.87 -	73.61]	< **0.001**
	Polyamines/choline	−30.56	[−46.38 -	−14.73]	< **0.001**
	Polyamines/creatine	18.56	[−1.41 -	38.53]	0.07
	MRSI ratio	41.88	[20.98 -	62.78]	< **0.001**
	ADC	−77.83	−104.25 -	−51.41]	< **0.001**

examining MRSI + DWI at 3 T, generating recursive partitioning trees for characterizing benign and malignant PZ regions, and evaluating the accuracy of PZ cancer identification in a test set. The AUCs we found for MRSI, DWI, and MRSI + DWI (of 0.82, 0.93, and 0.96, respectively) were higher than those found in the studies performed at 1.5 T: One of those studies found AUCs of 0.74, 0.81and 0.85 for MRSI, DWI, and MRSI + DWI, respectively [16]. In another study, for voxels containing ≥30% tumor, MRSI + DWI had an AUC of 0.81, which was similar to that of Cho/Cit (0.79) and better than that of DWI (i.e., ADC) alone (0.66); for voxels containing ≥70% tumor, Cho/Cit + ADC had significantly higher specificity compared with Cho/Cit alone and ADC alone [15]. Our MRSI findings are more consistent with those of a study performed at 3 T with a combination of external surface coil elements, in which MRSI had an AUC of 0.84 for the discrimination of benign and malignant PZ regions [12].

As noted by Chitkara et al., the understanding of metabolic patterns on MRSI and the rules for classifying them must be adapted to the field strength (1.5 T vs. 3 T) and to acquisition parameters such as TR and TE [21]. For spectroscopic imaging, the 3 T field strength provides higher SNR as well as higher metabolite resolution than does 1.5 T. Although all MRSI-measured values were available during the process, the recursive partitioning method incorporated only the MRSI ratio to distinguish benign from malignant lesions. In our study, polyamine information was assessed through measuring PA/Cho, PA/Cr, and MRSI ratio; this differs from the approach taken in the study by Shukla-Dave et al., which used a scoring system for the PA peak (in relation to the choline peak) and found that the PA peak played an important role in the identification of PZ prostate cancer at 1.5 T [10]. Ideally, a method should be developed that provides quantification of the concentrations of the metabolites [22], which would generate more precise, reliable metabolite estimates that are independent of acquisition parameters. In this study, however, we aimed to devise a classification system that could readily be extended to clinical use with the acquisition and post-processing tools provided by the manufacturer.

In addition to distinguishing choline from polyamine peaks, challenges to generating reliable metabolite estimates within a clinical

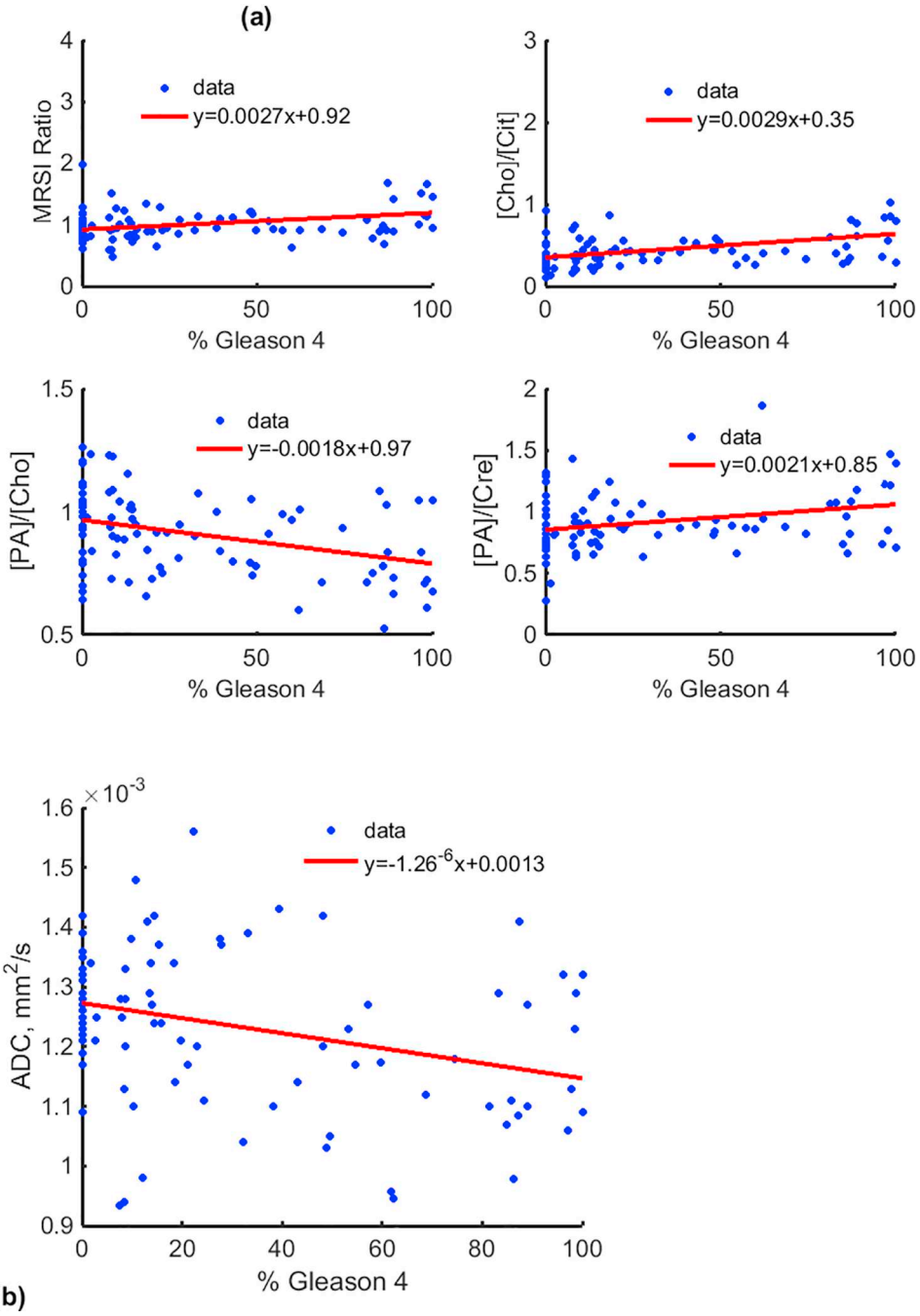

Fig. 7. (A) Scatter plots of mean MRSI parameters (MRSI ratio, [Cho]/[Cit], [PA]/[Cho], [PA]/[Cre]) and (B) mean ADC versus percentage of Gleason grade 4 tumor for all lesions in the analysis. Also included is the line of best fit.

setting include obtaining sufficient SNR, minimizing unwanted signal from fat and water, and addressing signal complications for citrate (and polyamines)—which can have timing dependencies due to *J*-coupling [23]. In this study we used the PROSE software for 3 T spectroscopic imaging provided by GE under a research agreement. A recent spectroscopic methodology review by Kobus et al. highlighted that TEs from three different vendors at 3 T are vastly different [3]. The metabolic ratios for the PZ in our study differed from those reported by others partly because of differences in acquisition parameters (such as TR and TE) as well as differences in sequence design and post-processing methods. The differences in reported values suggest a need to standardize acquisition parameters and sequence designs to make comparison across platforms feasible.

Presently, DWI is commonly integrated into clinical prostate MRI protocols in many institutions, in part because its acquisition times are short and it does not require the administration of contrast material. Findings regarding the value of adding DWI to T2-weighted imaging in the detection of prostate cancer vary; for example, one study found that the combination of DWI and T2-weighted imaging performed better than T2-weighted imaging alone in the detection of significant cancer (Gleason score ≥ 6 and diameter > 4 mm) in the PZ [24], while another study found that combined DWI and T2-weighted imaging performed similarly to T2-weighted imaging alone for the detection of tumor, although ADC values correlated significantly with prostate cancer aggressiveness [25]. A reporting system called PIRADS has been developed for the interpretation of multi-parametric MRI [1,26,27]. Although MRSI was included in the original PI-RADS, it was not included in the most recent version, PI-RADS 2.0. The limitations of MRSI

include a lack of standardized evaluation system, long examination times, and the need for expertise in interpretation of spectra. Characterizing benign and malignant PZ tissue at 3 T using MRSI could be useful for a number of future applications including chemoprevention trials which may rely on the assessment of metabolites (such as polyamines) in the prostate gland. Elevated polyamines characterized in-vivo in the prostate gland is a signature of healthy prostate tissue [28]. Recently it has been shown that ornithine decarboxylase enzyme in polyamine pathway is critical in prostate tumorigenesis [29].

We found that DWI alone had very good sensitivity (98%) with low specificity (51%). We also found that the specificity of MRSI in the detection of PZ cancer was good (82%); this is consistent with the results of a study performed at 1.5 T by Scheidler et al. [30], in which MRSI of definite cancer had reasonably good specificity (75%) but lower sensitivity (63%). Shukla-Dave et al. also found that MRSI analysis yielded good specificity (85%) but lower sensitivity (42%) [10]. Our results suggest that the combination of MRSI + DWI could simultaneously allow for both high sensitivity and specificity (in the test set, MRSI + DWI had sensitivity of 79% and specificity of 90%). However, caution must be used in interpreting our results, as this was a small sample retrospective study.

Recently, Sauter et al. investigated the utility of quantitative Gleason grading in prostate biopsies and prostatectomy specimens [31]. Their results, which suggested the potential utility of such grading, motivated us to measure the (continuous) percentage of Gleason grade ≥ 4 in prostatectomy specimens rather than the categorized Gleason score; the former approach allowed us to use GEE methods to examine the relationships of percentage of Gleason grade ≥ 4 disease to MRSI parameters and ADC within lesions. Our univariate analysis showed significant relationships of all the metabolic ratios and ADC with the percentage of Gleason score. Although we used equipment from a different manufacturer as well as different data acquisition software, our findings were comparable to those of Kobus et al. [32]; they found significant correlations between MRSI and DWI results at 3 T and aggressiveness classes (low-grade tumors were defined as tumors consisting of only Gleason grade 2 and/or 3 components; intermediate-grade tumors were defined as tumors that had a secondary or tertiary Gleason grade 4 component but no grade 5 component; and high-grade tumors were defined as tumors with a primary grade 4 component and/or a grade 5 component) [32]. Specifically, for PZ tumors, they found significant correlations between aggressiveness classes and maximum (Cho + Cr)/Cit, maximum Cho/Cr, and minimum 25th percentile ADC value [5,32]. In a separate study, they found that ADC and (citrate + spermine + creatine)/choline correlated positively with percentage area of lumen and correlated negatively with the percentage area of nuclei, suggesting that these aspects of tissue composition may influence the estimated MRSI parameters and ADC values [33].

Our study had several limitations. It was a single-institution study involving a limited number of patients, and the analyses were performed retrospectively. The vast majority of patients (56/67 [83.6%]) had a Gleason sum ≥3 + 4; furthermore, of the patients who gave consent to undergo the 3 T multi-parametric MRI exam incorporating MRSI, only those who underwent radical prostatectomy, had whole-mount step-section pathology available, and had tumors with volume > 0.1 cm^3 were included in our retrospective analysis. Therefore, the population of patients with low-risk prostate cancer was not fully represented, and extension of the findings to the general patient population requires care. Another limitation of our study was that our analysis of MRSI and DWI data was based on the acquisition and post-processing tools provided by the manufacturer, in part because we wished to assess the utility of MRSI and DWI within a clinical setting. Custom-made tools to enhance the quality of data acquisition, such as multiple b-value acquisition of DWI [34,35] or rapid MRSI acquisitions [36], as well as further analyses of the acquired data (e.g., modeling of multi-b-value diffusion data or quantitative spectroscopic analysis), could have added value in the detection of PZ tumors. Perhaps the major limitation of the current study is that the specificity of the techniques, particularly MRSI, are overestimated as compared to the clinical scenario. In this retrospective study, regions were selected based on prior knowledge of the location of the tumor. To establish the clinical utility of the proposed methods, a prospective multi-institutional study that includes all MRSI voxels and corresponding areas on ADC map within PZ should be performed to evaluate the sensitivity/specificity of the proposed classification rules.

In conclusion, we generated systems for characterizing benign and malignant PZ tissue at 3 T using MRSI, DWI, and MRSI + DWI, and we demonstrated the potential usefulness of combining MRSI and DWI information in the identification of prostate cancer in the PZ at 3 T. Further studies are required to assess the effectiveness of MRSI + DWI in the detection of prostate cancer in different patient populations.

Acknowledgments

We are grateful to Ada Muellner, MS, for helping to edit this manuscript.

Conflicts of interest and source of funding

Project funding was provided, in part, by the Office of Extramural Research, National Institutes of Health (US) (R01 CA76423).

Disclosures and conflict of interest

None.

References

[1] Weinreb JC, Barentsz JO, Choyke PL, Cornud F, Haider MA, Macura KJ, et al. PI-RADS prostate imaging - reporting and data system: 2015, Version 2. Eur Urol 2016;69(1):16–40.
[2] Padhani AR, Liu G, Koh DM, Chenevert TL, Thoeny HC, Takahara T, et al. Diffusion-weighted magnetic resonance imaging as a cancer biomarker: consensus and recommendations. Neoplasia 2009;11(2):102–25.
[3] Kobus T, Wright AJ, Scheenen TW, Heerschap A. Mapping of prostate cancer by 1H MRSI. NMR Biomed 2014;27(1):39–52.
[4] Kobus T, Wright AJ, Weiland E, Heerschap A, Scheenen TW. Metabolite ratios in 1H MR spectroscopic imaging of the prostate. Magn Reson Med 2015;73(1):1–12.
[5] Kobus T, Hambrock T, Hulsbergen-Van De Kaa CA, Wright AJ, Barentsz JO, Heerschap A, et al. In vivo assessment of prostate cancer aggressiveness using magnetic resonance spectroscopic imaging at 3 T with an endorectal coil. Eur Urol 2011;60(5):1074–80.
[6] Kurhanewicz J, Vigneron DB, Hricak H, Narayan P, Carroll P, Nelson SJ. Three-dimensional H-1 MR spectroscopic imaging of the in situ human prostate with high (0.24–0.7-cm^3) spatial resolution. Radiology 1996;198(3):795–805.
[7] Heerschap A, Jager GJ, van der Graaf M, Barentsz JO, Ruijs SH. Proton MR spectroscopy of the normal human prostate with an endorectal coil and a double spin-echo pulse sequence. Magn Reson Med 1997;37(2):204–13.
[8] Jung JA, Coakley FV, Vigneron DB, Swanson MG, Qayyum A, Weinberg V, et al. Prostate depiction at endorectal MR spectroscopic imaging: investigation of a standardized evaluation system. Radiology 2004;233(3):701–8.
[9] Futterer JJ, Scheenen TW, Heijmink SW, Huisman HJ, Hulsbergen-Van de Kaa CA, Witjes JA, et al. Standardized threshold approach using three-dimensional proton magnetic resonance spectroscopic imaging in prostate cancer localization of the entire prostate. Invest Radiol 2007;42(2):116–22.
[10] Shukla-Dave A, Hricak H, Moskowitz C, Ishill N, Akin O, Kuroiwa K, et al. Detection of prostate cancer with MR spectroscopic imaging: an expanded paradigm incorporating polyamines. Radiology 2007;245(2):499–506.
[11] Futterer JJ, Heijmink SW, Scheenen TW, Jager GJ, Hulsbergen-Van de Kaa CA, Witjes JA, et al. Prostate cancer: local staging at 3-T endorectal MR imaging–early experience. Radiology 2006;238(1):184–91.
[12] Scheenen TW, Heijmink SW, Roell SA, Hulsbergen-Van de Kaa CA, Knipscheer BC, Witjes JA, et al. Three-dimensional proton MR spectroscopy of human prostate at 3 T without endorectal coil: feasibility. Radiology 2007;245(2):507–16.
[13] Giskeodegard GF, Bertilsson H, Selnaes KM, Wright AJ, Bathen TF, Viset T, et al. Spermine and citrate as metabolic biomarkers for assessing prostate cancer aggressiveness. PLoS One 2013;8(4):e62375.
[14] Hegde JV, Mulkern RV, Panych LP, Fennessy FM, Fedorov A, Maier SE, et al. Multiparametric MRI of prostate cancer: an update on state-of-the-art techniques and their performance in detecting and localizing prostate cancer. J Magn Reson Imaging 2013;37(5):1035–54.
[15] Reinsberg SA, Payne GS, Riches SF, Ashley S, Brewster JM, Morgan VA, et al. Combined use of diffusion-weighted MRI and 1H MR spectroscopy to increase

accuracy in prostate cancer detection. AJR Am J Roentgenol 2007;188(1):91–8.
[16] Mazaheri Y, Shukla-Dave A, Hricak H, Fine SW, Zhang J, Inurrigarro G, et al. Prostate cancer: identification with combined diffusion-weighted MR imaging and 3D 1H MR spectroscopic imaging–correlation with pathologic findings. Radiology 2008;246(2):480–8.
[17] Schricker AA, Pauly JM, Kurhanewicz J, Swanson MG, Vigneron DB. Dualband spectral-spatial RF pulses for prostate MR spectroscopic imaging. Magn Reson Med 2001;46(6):1079–87.
[18] Chen AP, Cunningham CH, Kurhanewicz J, Xu D, Hurd RE, Pauly JM, et al. High-resolution 3D MR spectroscopic imaging of the prostate at 3 T with the MLEV-PRESS sequence. Magn Reson Imaging 2006;24(7):825–32.
[19] Coakley FV, Qayyum A, Kurhanewicz J. Magnetic resonance imaging and spectroscopic imaging of prostate cancer. J Urol 2003;170(6 Pt 2):S69–75. (discussion S-6).
[20] Seshan VE, Gonen M, Begg CB. Comparing ROC curves derived from regression models. Stat Med 2013;32(9):1483–93.
[21] Chitkara M, Westphalen A, Kurhanewicz J, Qayyum A, Poder L, Reed G, et al. Magnetic resonance spectroscopic imaging of benign prostatic tissue: findings at 3.0 T compared to 1.5 T-initial experience. Clin Imaging 2011;35(4):288–93.
[22] Garcia-Martin ML, Adrados M, Ortega MP, Fernandez Gonzalez I, Lopez-Larrubia P, Viano J, et al. Quantitative (1) H MR spectroscopic imaging of the prostate gland using LCModel and a dedicated basis-set: correlation with histologic findings. Magn Reson Med 2011;65(2):329–39.
[23] Trabesinger AH, Meier D, Dydak U, Lamerichs R, Boesiger P. Optimizing PRESS localized citrate detection at 3 Tesla. Magn Reson Med 2005;54(1):51–8.
[24] Haider MA, van der Kwast TH, Tanguay J, Evans AJ, Hashmi AT, Lockwood G, et al. Combined T2-weighted and diffusion-weighted MRI for localization of prostate cancer. AJR Am J Roentgenol 2007;189(2):323–8.
[25] Vargas HA, Akin O, Franiel T, Mazaheri Y, Zheng J, Moskowitz C, et al. Diffusion-weighted endorectal MR imaging at 3 T for prostate cancer: tumor detection and assessment of aggressiveness. Radiology 2011;259(3):775–84.
[26] Barentsz J, de Rooij M, Villeirs G, Weinreb J. Prostate imaging-reporting and data system version 2 and the implementation of high-quality prostate magnetic resonance imaging. Eur Urol 2017;72(2):189–91.
[27] Barentsz JO, Weinreb JC, Verma S, Thoeny HC, Tempany CM, Shtern F, et al. Synopsis of the PI-RADS v2 guidelines for multiparametric prostate magnetic resonance imaging and recommendations for use. Eur Urol 2016;69(1):41–9.
[28] Shukla-Dave A, Hricak H, Ishill NM, Moskowitz CS, Drobnjak M, Reuter VE, et al. Correlation of MR imaging and MR spectroscopic imaging findings with Ki-67, phospho-Akt, and androgen receptor expression in prostate cancer. Radiology 2009;250(3):803–12.
[29] Shukla-Dave A, Castillo-Martin M, Chen M, Lobo J, Gladoun N, Collazo-Lorduy A, et al. Ornithine decarboxylase is sufficient for prostate tumorigenesis via androgen receptor signaling. Am J Pathol 2016;186(12):3131–45.
[30] Scheidler J, Hricak H, Vigneron DB, Yu KK, Sokolov DL, Huang LR, et al. Prostate cancer: localization with three-dimensional proton MR spectroscopic imaging—clinicopathologic study. Radiology 1999;213(2):473–80.
[31] Sauter G, Steurer S, Clauditz TS, Krech T, Wittmer C, Lutz F, et al. Clinical utility of quantitative Gleason grading in prostate biopsies and prostatectomy specimens. Eur Urol 2016;69(4):592–8.
[32] Kobus T, Vos PC, Hambrock T, De Rooij M, Hulsbergen-Van de Kaa CA, Barentsz JO, et al. Prostate cancer aggressiveness: in vivo assessment of MR spectroscopy and diffusion-weighted imaging at 3 T. Radiology 2012;265(2):457–67.
[33] Kobus T, van der Laak JA, Maas MC, Hambrock T, Bruggink CC, Hulsbergen-van de Kaa CA, et al. Contribution of histopathologic tissue composition to quantitative MR spectroscopy and diffusion-weighted imaging of the prostate. Radiology 2016;278(3):801–11. (142889).
[34] deSouza NM, Riches SF, Vanas NJ, Morgan VA, Ashley SA, Fisher C, et al. Diffusion-weighted magnetic resonance imaging: a potential non-invasive marker of tumour aggressiveness in localized prostate cancer. Clin Radiol 2008;63(7):774–82.
[35] Riches SF, Hawtin K, Charles-Edwards EM, de Souza NM. Diffusion-weighted imaging of the prostate and rectal wall: comparison of biexponential and monoexponential modelled diffusion and associated perfusion coefficients. NMR Biomed 2009;22(3):318–25.
[36] Cunningham CH, Vigneron DB, Chen AP, Xu D, Nelson SJ, Hurd RE, et al. Design of flyback echo-planar readout gradients for magnetic resonance spectroscopic imaging. Magn Reson Med 2005;54(5):1286–9.